A Lagrangian subgrid-scale model with dynamic estimation of Lagrangian time scale for large eddy simulation of complex flows

Aman Verma and Krishnan Mahesh
Department of Aerospace Engineering and Mechanics, University of Minnesota, Minneapolis, Minnesota 55455, USA

(Received 21 November 2011; accepted 14 June 2012; published online 3 August 2012)

The dynamic Lagrangian averaging approach for the dynamic Smagorinsky model for large eddy simulation is extended to an unstructured grid framework and applied to complex flows. The Lagrangian time scale is dynamically computed from the solution and does not need any adjustable parameter. The time scale used in the standard Lagrangian model contains an adjustable parameter θ. The dynamic time scale is computed based on a "surrogate-correlation" of the Germano-identity error (GIE). Also, a simple material derivative relation is used to approximate GIE at different events along a pathline instead of Lagrangian tracking or multi-linear interpolation. Previously, the time scale for homogeneous flows was computed by averaging along directions of homogeneity. The present work proposes modifications for inhomogeneous flows. This development allows the Lagrangian averaged dynamic model to be applied to inhomogeneous flows without any adjustable parameter. The proposed model is applied to LES of turbulent channel flow on unstructured zonal grids at various Reynolds numbers. Improvement is observed when compared to other averaging procedures for the dynamic Smagorinsky model, especially at coarse resolutions. The model is also applied to flow over a cylinder at two Reynolds numbers and good agreement with previous computations and experiments is obtained. Noticeable improvement is obtained using the proposed model over the standard Lagrangian model. The improvement is attributed to a physically consistent Lagrangian time scale. The model also shows good performance when applied to flow past a marine propeller in an off-design condition; it regularizes the eddy viscosity and adjusts locally to the dominant flow features. © *2012 American Institute of Physics*. [http://dx.doi.org/10.1063/1.4737656]

I. BACKGROUND

High Reynolds number flows of practical importance exhibit such a large range of length and time scales that direct numerical simulations (DNS) are rendered impossible for the foreseeable future. Large eddy simulation (LES) is a viable analysis and design tool for complex flows due to advances in massive parallel computers and numerical techniques. LES is essentially an under-resolved turbulence simulation using a model for the subgrid-scale (SGS) stress to account for the inter-scale interaction between the resolved and the unresolved scales. The success of LES is due to the dominance of the large, geometry dependent, resolved scales in determining important flow dynamics and statistics.

In LES, the large scales are directly accounted for by the spatially, temporally, or spatio-temporally filtered Navier-Stokes equations and the small scales are modeled. The spatially filtered incompressible Navier-Stokes equations are

$$\frac{\partial \overline{u}_i}{\partial t} + \frac{\partial}{\partial x_j}(\overline{u}_i \overline{u}_j) = -\frac{\partial \overline{p}}{\partial x_i} + \nu \frac{\partial^2 \overline{u}_i}{\partial x_j \partial x_j} - \frac{\partial \tau_{ij}}{\partial x_j},$$
$$\frac{\partial \overline{u}_i}{\partial x_i} = 0, \tag{1}$$

where x_i denotes the spatial coordinates, u_i is the velocity field, p is the pressure, ν is the kinematic viscosity, $\overline{()}$ denotes the spatial filter at scale Δ, and $\tau_{ij} = \overline{u_i u_j} - \overline{u}_i \overline{u}_j$ is the SGS stress.

It is generally assumed that small scales are more universal and isotropic than large scales; eddy viscosity type SGS models are therefore widely used in LES. The original Smagorinsky model[1] is a simple model for the SGS stress in terms of the local resolved flow,

$$\tau_{ij} - \frac{1}{3}\tau_{kk}\delta_{ij} = -2(C_s\Delta)^2 |\overline{S}| \overline{S}_{ij} = -2\nu_t \overline{S}_{ij}, \tag{2}$$

where C_s is a model coefficient, Δ is the filter width, $\overline{S}_{ij}$ is the strain rate tensor, $|\overline{S}| = (2\overline{S}_{ij}\overline{S}_{ij})^{1/2}$, and $\nu_t = (C_s\Delta)^2|\overline{S}|$ is the eddy-viscosity.

In the original Smagorinsky model, C_s is assumed to be a global adjustable parameter. The dynamic Smagorinsky model (DSM)[2] removes this limitation by dynamically computing the model coefficient from the resolved flow and allowing it to vary in space and time. DSM is based on the Germano identity,

$$L_{ij} = T_{ij} - \widehat{\tau}_{ij}, \tag{3}$$

where

$$L_{ij} = \widehat{\overline{u}_i \overline{u}_j} - \widehat{\overline{u}}_i \widehat{\overline{u}}_j, \qquad T_{ij} = \widehat{\overline{u_i u_j}} - \widehat{\overline{u}}_i \widehat{\overline{u}}_j, \quad \text{and} \quad \widehat{\tau}_{ij} = \widehat{\overline{u_i u_j}} - \widehat{\overline{u}_i \overline{u}_j}. \tag{4}$$

Here, $\widehat{()}$ denotes test filtering at scale $\widehat{\Delta}$ and is usually taken to be $\widehat{\Delta} = 2\Delta$. T_{ij} is analogous to τ_{ij} and is the corresponding SGS stress at the test filter scale. L_{ij} is the stress due to scales intermediate between Δ and 2Δ and can be computed directly from the resolved field. The deviatoric parts (denoted by $()^d$) of τ_{ij} and T_{ij} are modeled by using the Smagorinsky model at scales Δ and $\widehat{\Delta}$ as

$$\tau_{ij} - \frac{1}{3}\tau_{kk}\delta_{ij} = -2(C_s\Delta)^2|\overline{S}|\overline{S}_{ij} \quad \text{and} \quad T_{ij} - \frac{1}{3}T_{kk}\delta_{ij} = -2(C_s\widehat{\Delta})^2|\widehat{\overline{S}}|\widehat{\overline{S}}_{ij}. \tag{5}$$

The dynamic procedure to obtain the SGS model coefficient C_s attempts to minimize the Germano-identity error (GIE),

$$\begin{aligned}\epsilon_{ij} &= T^d_{ij} - \widehat{\tau}^d_{ij} - L^d_{ij} \\ &= 2(C_s\Delta)^2 \left[\widehat{|\overline{S}|\overline{S}_{ij}} - \left(\frac{\widehat{\Delta}}{\Delta}\right)^2 |\widehat{\overline{S}}|\widehat{\overline{S}}_{ij} \right] - L^d_{ij} \\ &= (C_s\Delta)^2 M_{ij} - L^d_{ij},\end{aligned} \tag{6}$$

where $M_{ij} = 2\left[\widehat{|\overline{S}|\overline{S}_{ij}} - \left(\frac{\widehat{\Delta}}{\Delta}\right)^2 |\widehat{\overline{S}}|\widehat{\overline{S}}_{ij}\right]$.

Since $\epsilon_{ij}(C_s) = 0$ is a tensor equation, C_s is over determined. The original DSM due to Germano *et al.*[2] satisfies $\epsilon_{ij}S_{ij} = 0$ to obtain C_s. Lilly[3] found the equations to be better behaved when minimizing ϵ_{ij} in a least-square sense, yielding

$$(C_s\Delta)^2 = \frac{\langle L_{ij} M_{ij} \rangle}{\langle M_{ij} M_{ij} \rangle}, \tag{7}$$

where $\langle \cdot \rangle$ denotes averaging over homogeneous direction(s).

Without any kind of averaging, the local dynamic model is known to predict a highly variable eddy viscosity field. More so, the eddy viscosity can be negative, which causes solutions to become unstable. It was found that C_s has a large auto-correlation time which caused negative eddy viscosity to persist for a long time, thereby causing a divergence of the total energy.[4] Hence averaging and/or clipping C_s (setting negative values of C_s to 0) was found to be necessary to stabilize the model. Positive C_s from Eq. (7) provides dissipation thereby ensuring the transfer of energy

from the resolved to the subgrid scales. Also, clipping is almost never required when averaging over homogenous directions. Ghosal *et al.*[5] showed this averaging and/or clipping operation to be essentially a constrained minimization of Eq. (6).

However, the requirement of averaging over at least one homogeneous direction is impractical for complex inhomogeneous flows. To circumvent the problems of lack of homogeneous direction(s) and undesirable clipping, Ghosal *et al.*[5] proposed a "dynamic localization model (k-equation)" to allow for backscatter by including an equation for subgrid scale kinetic energy budget. Ghosal's formulation entails further computational expense as well as additional model coefficients. To enable averaging in inhomogeneous flows, Meneveau *et al.*[6] developed a Lagrangian version of DSM (LDSM) where C_s is averaged along fluid trajectories. Lagrangian averaging is physically appealing considering the Lagrangian nature of the turbulence energy cascade.[7,8]

In essence, the Lagrangian DSM attempts to minimize the pathline average of the local GIE squared. The objective function to be minimized is given by

$$E = \int_{pathline} \epsilon_{ij}(\mathbf{z})\epsilon_{ij}(\mathbf{z})d\mathbf{z} = \int_{-\infty}^{t} \epsilon_{ij}(\mathbf{z}(t'),t')\epsilon_{ij}(\mathbf{z}(t'),t')W(t-t')dt', \tag{8}$$

where $\mathbf{z}$ is the trajectory of a fluid particle for earlier times $t' < t$ and W is a weighting function to control the relative importance of events near time t, with those at earlier times.

Choosing the time weighting function of the form $W(t-t') = T^{-1}e^{-(t-t')/T}$ yields two transport equations for the Lagrangian average of the tensor products $L_{ij}M_{ij}$ and $M_{ij}M_{ij}$ as $\mathcal{I}_{LM}$ and $\mathcal{I}_{MM}$, respectively:

$$\begin{aligned} \frac{D\mathcal{I}_{LM}}{Dt} &\equiv \frac{\partial \mathcal{I}_{LM}}{\partial t} + \overline{u}_i \frac{\partial \mathcal{I}_{LM}}{\partial x_i} = \frac{1}{T}\left(L_{ij}M_{ij} - \mathcal{I}_{LM}\right) \quad \text{and} \\ \frac{D\mathcal{I}_{MM}}{Dt} &\equiv \frac{\partial \mathcal{I}_{MM}}{\partial t} + \overline{u}_i \frac{\partial \mathcal{I}_{MM}}{\partial x_i} = \frac{1}{T}\left(M_{ij}M_{ij} - \mathcal{I}_{MM}\right), \end{aligned} \tag{9}$$

whose solutions yield

$$(C_s\Delta)^2 = \frac{\mathcal{I}_{LM}}{\mathcal{I}_{MM}}. \tag{10}$$

Here T is a time scale which represents the "memory" of the Lagrangian averaging. Meneveau *et al.*[6] proposed the following time scale:

$$T = \theta\Delta(\mathcal{I}_{LM}\mathcal{I}_{MM})^{(-1/8)}; \qquad \theta = 1.5. \tag{11}$$

This procedure for Lagrangian averaging has also been extended to the scale-similar model by Anderson and Meneveau[9] and Sarghini *et al.*[10] and the scale-dependent dynamic model by Stoll and Porté-Agel.[11]

Note that the time scale for Lagrangian averaging in Eq. (11) contains an adjustable parameter which is typically chosen to be $\theta = 1.5$. The need for a "dynamic" Lagrangian time scale is motivated in Sec. II. Park and Mahesh[12] introduced a procedure for computing a dynamic Lagrangian time scale. However, the Park and Mahesh[12] formulation was in the context of a spectral structured solver, and considered their dynamic Lagrangian time scale model along with their proposed control-based corrected DSM. They proposed a correction step to compute the eddy viscosity using Fréchet derivatives, leading to further reduction of the Germano-identity error. Computing Fréchet derivatives of the objective function (in this case, the GIE) can involve significant computational overhead in an unstructured solver. The present work considers the dynamic Lagrangian time scale model in the absence of control-based corrections. Also, Park and Mahesh[12] computed their time scale for isotropic turbulence and turbulent channel flow by averaging along directions of homogeneity. The present work considers the time scale model in the absence of any spatial averaging.

The extension of the Lagrangian averaged DSM with a dynamic time scale to an unstructured grid framework requires modifications to the model proposed by Park and Mahesh[12] and is described in Sec. II A. The Lagrangian DSM with this dynamic time scale T_{SC} is applied to three problems—turbulent channel flow (Sec. IV A), flow past a cylinder (Sec. IV B), and flow past a marine propeller in an off-design condition (Sec. IV C), on unstructured grids at different Reynolds numbers. It is shown

that the procedure works well on unstructured grids and shows improvement over existing averaged DSM methods. Sections IV A 2 to IV A 4 discuss the variation of T_{SC} with grid resolution, Reynolds numbers, and the practical advantages of this procedure in ensuring positive eddy viscosities and negligible computational overhead. Differences in the performance of the dynamic time scale and the original time scale due to Meneveau *et al.*[6] for the cylinder flow are analyzed in Sec. IV B 5. In Sec. IV C, the model is applied to a challenging complex flow and it is shown that T_{SC} is a physically consistent time scale whose use yields good results.

II. DYNAMIC LAGRANGIAN TIME SCALE

The time scale for Lagrangian averaging proposed by Meneveau *et al.* (henceforth, T_{LDSM}) contains an adjustable parameter which is typically chosen to be $\theta = 1.5$. This value was chosen based on the autocorrelation of $L_{ij}M_{ij}$ and $M_{ij}M_{ij}$ from DNS of forced isotropic turbulence. This arbitrariness is acknowledged to be undesirable by the authors and infact they document results of turbulent channel flow at $Re_\tau = 650$ to be marginally sensitive to the value of θ, with $\theta = 1.5$ appearing to yield the best results. You *et al.*[13] tested three different values of the relaxation factor θ and concluded T_{LDSM} was "reasonably robust" to the choice of θ for a $Re_\tau = 180$ channel flow. Over the years, choosing a value for θ has demanded significant consideration by many practitioners who have found the results to be sensitive to θ, especially in complex flows.[14]

The extension of the Lagrangian averaging procedure to other models has also presented the same dilemma. In simulations of turbulent channel flow at $Re_\tau = 1050$ using a two-coefficient Lagrangian mixed model,[9] Sarghini *et al.*[10] note that a different parameter in T_{LDSM} might be required for averaging the scale similar terms. Vasilyev *et al.*[15] proposed extensions to the Lagrangian dynamic model for a wavelet based approach and used $\theta = 0.75$ for incompressible isotropic turbulence.

Park and Mahesh[12] note that T_{LDSM} has a high dependence on the strain rate through the L_{ij} and M_{ij} terms. They however show that the time scale of the GIE near the wall and the channel centerline are similar. Thereby they argue that strain rate may not be the most appropriate quantity for defining a time scale for Lagrangian averaging of the GIE. It seems only natural that the averaging time scale should be the time scale of the quantity being averaged which in this case is the GIE. Park and Mahesh,[12] therefore, proposed a dynamic time scale T_{SC} called "surrogate-correlation based time scale" T_{SC}.

A. Surrogate-correlation based time scale

Assuming knowledge of the local and instantaneous values of the GIE squared ($\mathcal{E} = \epsilon_{ij}\epsilon_{ij}$) at five consecutive events along a pathline as shown in Fig. 1, where

$$\mathcal{E}^0 = \mathcal{E}(\mathbf{x}, t), \qquad \mathcal{E}^{\pm 1} = \mathcal{E}(\mathbf{x} \pm \mathbf{u}\Delta t, t \pm \Delta t), \qquad \mathcal{E}^{\pm 2} = \mathcal{E}(\mathbf{x} \pm 2\mathbf{u}\Delta t, t \pm 2\Delta t). \tag{12}$$

At each location, the following surrogate Lagrangian correlations for three separation times (0, Δt, $2\Delta t$) can be defined:

$$\mathcal{C}(l\Delta t) = \frac{1}{5-l}\sum_{k=-2}^{2-l}(\mathcal{E}^k - \overline{\mathcal{E}})(\mathcal{E}^{k+l} - \overline{\mathcal{E}}); \qquad (l = 0, 1, 2),$$
$$\text{where} \quad \overline{\mathcal{E}} = \frac{1}{5}\sum_{k=-2}^{2}\mathcal{E}^k \quad \text{is the average value.} \tag{13}$$

To increase the number of samples, Park and Mahesh[12] averaged $\mathcal{C}(l\Delta t)$ and $\overline{\mathcal{E}}$ along directions of homogeneity. This is not practical for extension to inhomogenous flows on unstructured grids. No further averaging of $\overline{\mathcal{E}}$ is a straightforward option; however, this approach results in a negative value for $\mathcal{C}(2\Delta t)$ and constant value for T_{SC} (not shown), which is unacceptable. To alleviate this, a

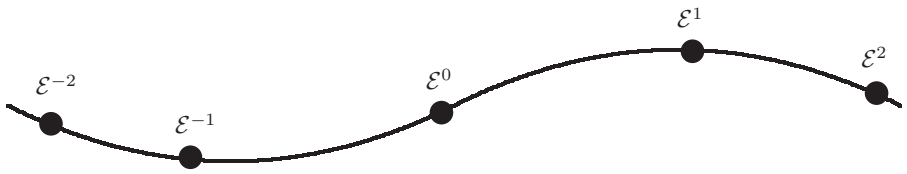

FIG. 1. $\epsilon_{ij}\epsilon_{ij}$ at five events along a pathline.

running time average of the above terms up to the current time t_n is computed:

$$\mathcal{C}(l\Delta t) = \sum_{t=0}^{t_n}\left(\frac{1}{5-l}\sum_{k=-2}^{2-l}(\mathcal{E}^{k,t}-\overline{\mathcal{E}}^{t})(\mathcal{E}^{k+l,t}-\overline{\mathcal{E}}^{t})\right); \qquad (l=0,1,2),$$
$$\text{where} \quad \overline{\mathcal{E}}^{t} = \sum_{\tau=0}^{t_n}\left(\frac{1}{5}\sum_{k=-2}^{2}\mathcal{E}^{k,\tau}\right) \quad \text{is the average value.} \tag{14}$$

This leads to converged correlations after sufficiently long times and is a consistent and general method to compute the surrogate Lagrangian correlations. These correlations are then normalized by the zero-separation correlation $\mathcal{C}(0)$ to obtain

$$\rho(0)=1, \qquad \rho(\Delta t)=\frac{\mathcal{C}(\Delta t)}{\mathcal{C}(0)}, \qquad \rho(2\Delta t)=\frac{\mathcal{C}(2\Delta t)}{\mathcal{C}(0)}. \tag{15}$$

An osculating parabola can be constructed passing through these three points and it can be described by

$$\rho(\delta t) = a(\delta t)^2 + b(\delta t) + 1, \tag{16}$$

where a, b can be written in terms of $\rho(0)=1$, $\rho(\Delta t)$, $\rho(2\Delta t)$, and Δt. Note that $\rho(\delta t)$ is an approximate correlation function (of separation time δt) for the true Lagrangian correlation. Thus the time scale based on the surrogate correlation T_{SC} is defined as the time when $\rho(\delta t)=0$, i.e., the positive solution

$$T_{SC} = \frac{-b-\sqrt{b^2-4a}}{2a}. \tag{17}$$

If the surrogate Lagrangian correlations $\mathcal{C}$ have enough samples, $1>\rho(\Delta t)>\rho(2\Delta t)$ is satisfied which leads to $a<0$. As a result, T_{SC} is always positive. In the initial stages of a simulation, there are not enough time samples. $1>\rho(\Delta t)>\rho(2\Delta t)$ may not be satisfied and a could be positive. In such cases, T_{SC} is obtained by constructing the osculating parabola to be of the form $1+a(\delta t)^2$ and passing through either of the two points $\rho(\Delta t)$, $\rho(2\Delta t)$:

$$T_{SC} = \min\left(\frac{dt}{\sqrt{1-\rho(\Delta t)}}, \frac{2dt}{\sqrt{1-\rho(2\Delta t)}}\right). \tag{18}$$

The minimum of the time scales is chosen so that the solution has lesser dependence on past values and can evolve faster from the initial transient stage. Note that the true Lagrangian correlation can be modeled by an exponential function $f(\delta t)=e^{(-\delta t/T)^2}$. Assuming $\Delta t \ll T$ and that $f(\delta t)$ passes through $\rho(0)=1$, $\rho(\Delta t)$, $\rho(2\Delta t)$, then $T_{SC}=\delta t=T$ is also the time when the modeled exponential correlation becomes e^{-1}.

B. Lagrangian approximation

The proposed dynamic time scale requires the values of the GIE squared $\mathcal{E}$ at five events along a pathline. Rovelstad *et al.*[16] and Choi *et al.*[8] suggest the use of Hermite interpolation for computing turbulent Lagrangian statistics. However, Hermite interpolation requires third order derivatives in every direction of the tracked quantity, rendering it prohibitively expensive. Meneveau *et al.*[6] use

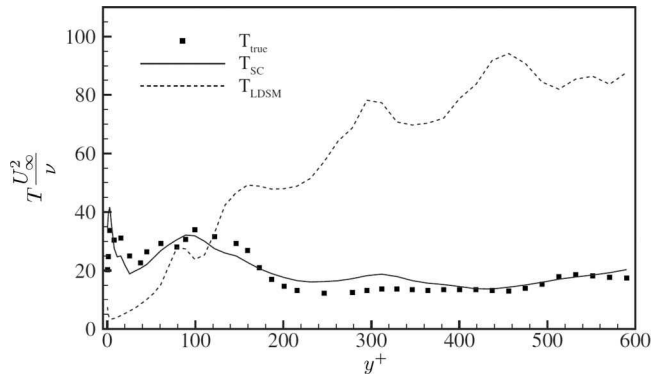

FIG. 2. Lagrangian time scales of the GIE for turbulent channel flow at $Re_\tau = 590$. Reproduced with permission from N. Park and K. Mahesh, Phys. Fluids **21**, 065106 (2009). Copyright © 2009 American Institute of Physics.

multilinear interpolation to obtain the values of $\mathcal{I}_{LM}$ and $\mathcal{I}_{MM}$ at a Lagrangian location. Even multilinear interpolation gets expensive in an unstructured grid setting. The use of an expensive interpolation method just to compute the time scale for Lagrangian averaging may be unnecessary. As a result, a simple material derivative relation as proposed by Park and Mahesh[12] is used to approximate Lagrangian quantities in an Eulerian framework,

$$\frac{D\mathcal{E}}{Dt} = \frac{\partial \mathcal{E}}{\partial t} + \overline{u}_i \frac{\partial \mathcal{E}}{\partial x_i}. \tag{19}$$

A simple first order in time and central second order in space, finite-volume approximation for the convective term is used to approximate values of $\mathcal{E}$ in Eq. (12) in terms of the local $\mathcal{E}(\mathbf{x}, t) = \mathcal{E}^{0,n}$ and $\mathcal{E}(\mathbf{x}, t - \Delta t) = \mathcal{E}^{0,n-1}$. The Green-Gauss theorem is used to express the convective term in conservative form and evaluate it as a sum over the faces of a computational volume.

Park and Mahesh[12] show that the dynamic time scale T_{SC} agrees well with the true Lagrangian correlation time scale, whereas T_{LDSM} exhibits opposite behavior near the wall (Fig. 2). They also show that the Lagrangian correlations at different wall normal locations collapse when normalized with T_{SC} while such collapse is not observed with T_{LDSM}.

III. NUMERICAL METHOD

Equation (1) is solved by a numerical method developed by Mahesh *et al.*[17] for incompressible flows on unstructured grids. The algorithm is derived to be robust without numerical dissipation. It is a finite volume method where the Cartesian velocities and pressure are stored at the centroids of the cells and the face normal velocities are stored independently at the centroids of the faces. A predictor-corrector approach is used. The predicted velocities at the control volume centroids are first obtained and then interpolated to obtain the face normal velocities. The predicted face normal velocity is projected so that the continuity equation in Eq. (1) is discretely satisfied. This yields a Poisson equation for pressure which is solved iteratively using a multigrid approach. The pressure field is used to update the Cartesian control volume velocities using a least-square formulation. Time advancement is performed using an implicit Crank-Nicolson scheme. The algorithm has been validated for a variety of problems over a range of Reynolds numbers.[17] To improve results on skewed grids, the viscous terms and the pressure Poisson equation are treated differently. The generalized improved deferred correction method by Jang[18] is used to calculate the viscous derivatives and the right-hand side of the pressure Poisson equation.

IV. RESULTS

The Lagrangian DSM with dynamic time scale T_{SC} is applied to three problems: turbulent channel flow (Sec. IV A), flow past a cylinder (Sec. IV B), and flow past a marine propeller in an off-design condition called crashback (Sec. IV C).

TABLE I. Grid parameters for turbulent channel flow.

Case	Re_τ	$N_x \times N_y \times N_z$	$L_x/\delta \times L_z/\delta$	Δx^+	Δz^+	$\Delta y^+_{\min}$	$\Delta y_{cen}/\delta$
			LES				
590f	590	$160 \times 150 \times 200$	$2\pi \times \pi$	23.2	9.3	1.8	0.03
590tl		$160 \times 84 \times (200, 100)$		23.2	9.3,18.5	1.8	0.04
590c		$64 \times 64 \times 64$		58	29	1.6	0.08
1ktl	1000	$160 \times 84 \times (200, 100)$		39.3	15.8,31.4	3.1	0.04
2ktl	2000	$320 \times 120 \times (400, 200, 100)$		39.3	15.7,31.4,62.8	2.0	0.04
			DNS				
Reference 19	587	$384 \times 257 \times 384$	$2\pi \times \pi$	9.7	4.8	...	0.012
Reference 20	934	$384 \times 385 \times 384$	$8\pi \times 3\pi$	11	5.7	...	...
Reference 21	2003	$384 \times 633 \times 384$	$8\pi \times 3\pi$	12	6.1	...	...

A. Turbulent channel flow

Results are shown for a turbulent channel flow at three Reynolds numbers; $Re_\tau = 590$, 1000, 2000, and different grid resolutions. Here $Re_\tau = u_\tau \delta/\nu$ where u_τ, δ, and ν denote the friction velocity, channel half-width, and viscosity, respectively. Table I lists the Re_τ and grid distribution for the various simulations. All LES have uniform spacing in x. The cases with "tl" indicate that a 4:2 transition layer has been used in z along y as shown in Fig. 3. As shown, a transition layer allows transition between two fixed edge ratio computational elements. It allows a finer wall spacing to coarsen to a fixed ratio coarser outer region spacing. All other cases have a uniform spacing in z. The LES results are compared to the DNS of Moser *et al.*[19] for $Re_\tau = 590$, Alamo *et al.*[20] for $Re_\tau = 1000$, and Hoyas and Jimenez[21] for $Re_\tau = 2000$ whose grid parameters are also included in the table for comparison. Note that the LES have employed noticeably coarse resolutions and hence contribution from the SGS model is expected to be significant. Consequently, the performance and dependence of T_{SC} is discussed in Secs. IV A 1–IV A 4.

1. Validation at $Re_\tau = 590$

Figure 4(a) shows good agreement for the mean velocity which indicates that the wall stress is well predicted. The velocity fluctuations in Fig. 4(b) are in reasonable agreement with unfiltered DNS as is to be expected at coarse resolutions. The Lagrangian DSM is active at this resolution and ν_t/ν peaks at 0.21 around $y^+ \sim 76$ (not shown). Figure 4(c) compares the dynamic Lagrangian time scale T_{SC} to T_{LDSM} which is calculated *a posteriori*. Note that T_{SC} is much higher near the wall than T_{LDSM}. Since T_{SC} is calculated from $\rho(\delta t)$, this behavior is consistent with the high correlation of

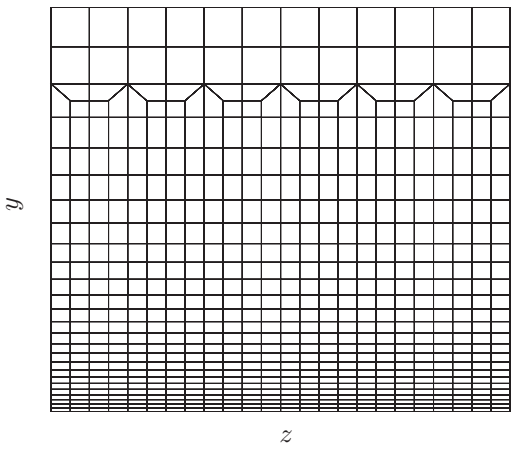

FIG. 3. Transition layer.

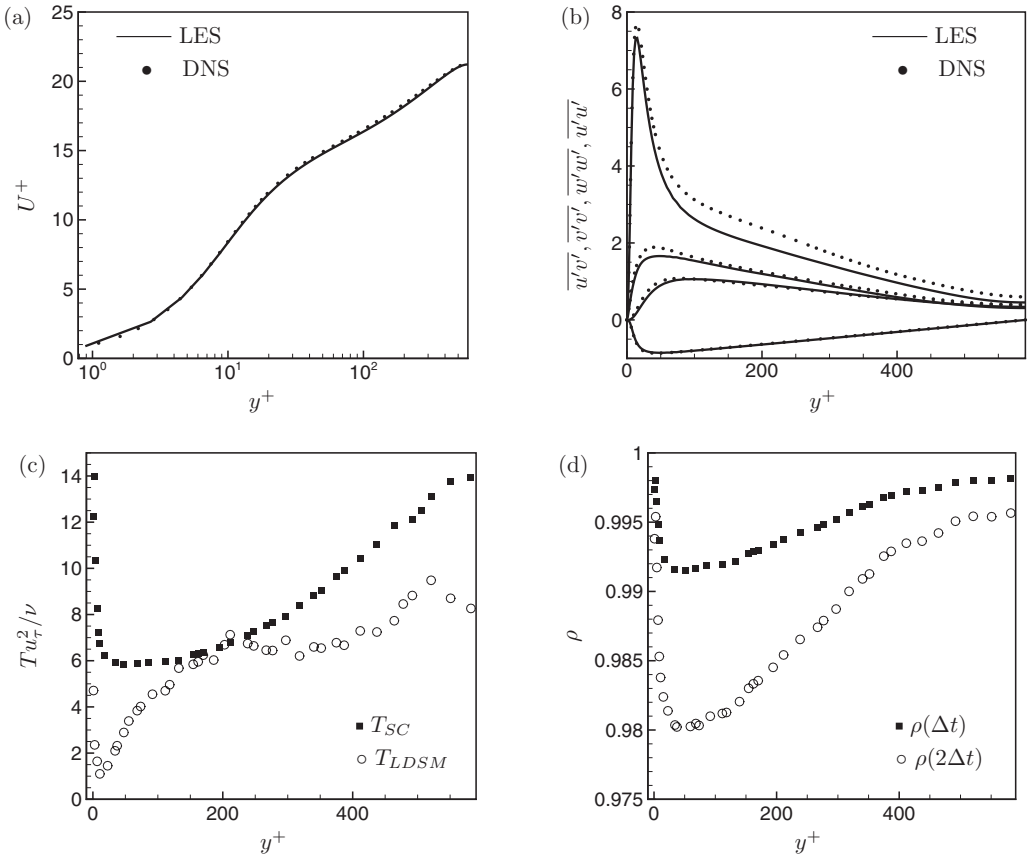

FIG. 4. Turbulent channel flow. Case 590f: (a) mean velocity, (b) rms velocity fluctuations, (c) time scales, and (d) normalized surrogate Lagrangian correlations.

GIE near the wall observed from Fig. 4(d). For such relatively coarse near-wall resolution, GIE is expected to be high near the wall and in addition, remain correlated longer because of the near-wall streaks. Figures 5(a) and 5(b) show that GIE is high near the wall in the form of near-wall streaks. Such behavior is consistent with the physical nature of the flow; the DNS of Choi *et al.*[8] shows higher streamwise Lagrangian time scale near the wall due to streaks and streamwise vortices.

Next, an unstructured zonal grid is used, which has a transition layer in Z along Y (case 590tl). Figures 6(a) and 6(b) show that the results are in good agreement, similar to case 590f. The statistics (Fig. 6(b)) have a small kink around $y^+ \sim 140$ where the grid transitions. This kink in the statistics is an artifact of numerical discretization and grid skewness, and is present even when no SGS model

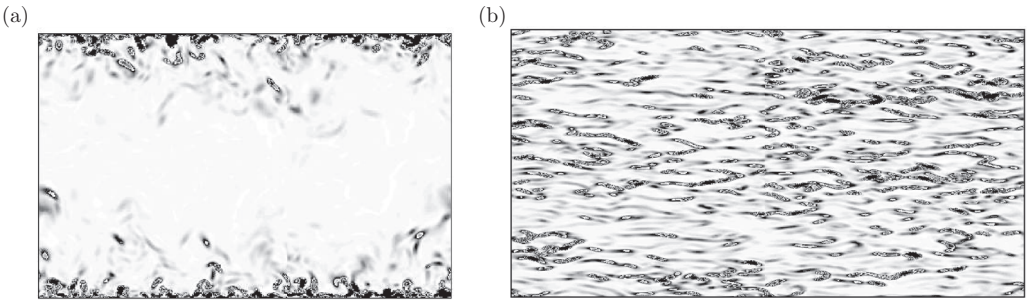

FIG. 5. Turbulent channel flow. Case 590f: instantaneous contours of Germano-identity error $g = (\text{GIE}/u_\tau^2)^2$, (a) yz plane, contours vary as $0 \le g \le 3$, (b) xz plane at $y^+ = 12$, contours vary as $0 \le g \le 40$.

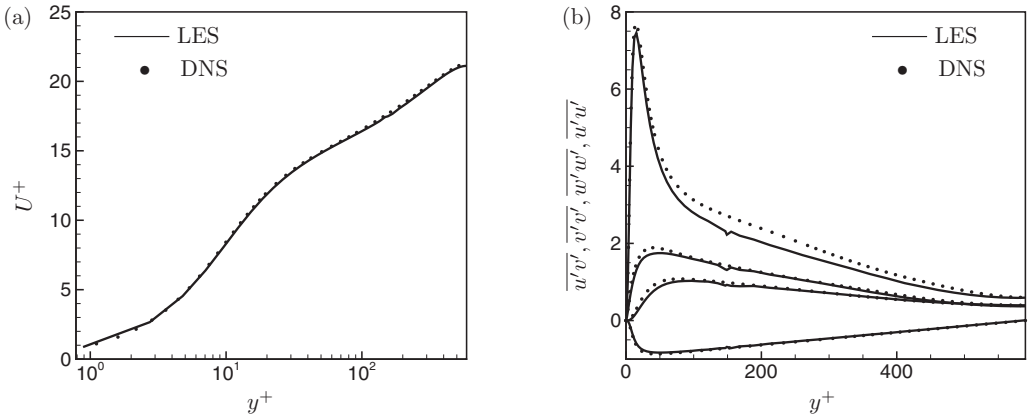

FIG. 6. Turbulent channel flow. Case 590tl : (a) mean velocity and (b) rms velocity fluctuations.

is used. Overall, the results indicate that the Lagrangian DSM with T_{SC} works well on a grid where non-orthogonal elements are present and plane averaging is not straightforward.

2. Variation with grid resolution at $Re_\tau = 590$

Figures 7(a) and 7(b) provide an interesting insight into the variation of T_{SC} and ν_t with grid resolution. The coarsest grid (590c) has the highest GIE (not shown) and consequently, highest T_{SC}. The SGS model compensates for the coarse grid by increasing ν_t. Cases 590f and 590tl have almost the same near-wall grid resolution. As a result, T_{SC} and ν_t are similar for the two cases until $y^+ \sim 50$. The y-distribution then begins to change slightly but the biggest change is in Δz which doubles due to the transition layer in case 590tl. The GIE also increases in the coarse region which subsequently increases the GIE correlations, resulting in higher T_{SC}.

3. Variation of T_{SC} with Reynolds numbers

The Lagrangian DSM with dynamic time scale T_{SC} (Eq. (17)) is applied to turbulent channel flow at higher Reynolds numbers of $Re_\tau = 1000$ and $Re_\tau = 2000$. The grid used for case 1ktl is the same as used for case 590tl and hence the resolution in wall units is almost twice as coarse, as shown in Table I. Figure 8(a) shows good agreement for the mean velocity which indicates that the wall stress is well predicted. The velocity fluctuations in Fig. 8(b) are in reasonable agreement with unfiltered DNS. The grid used for case 2ktl is based on similar scaling principles as case 590tl,

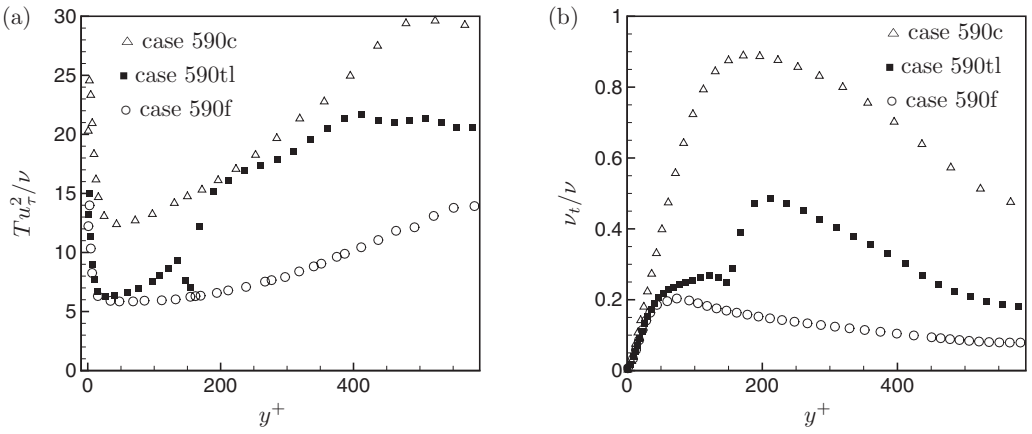

FIG. 7. Turbulent channel flow. Comparison of (a) Lagrangian time scales T_{SC} and (b) eddy viscosity.

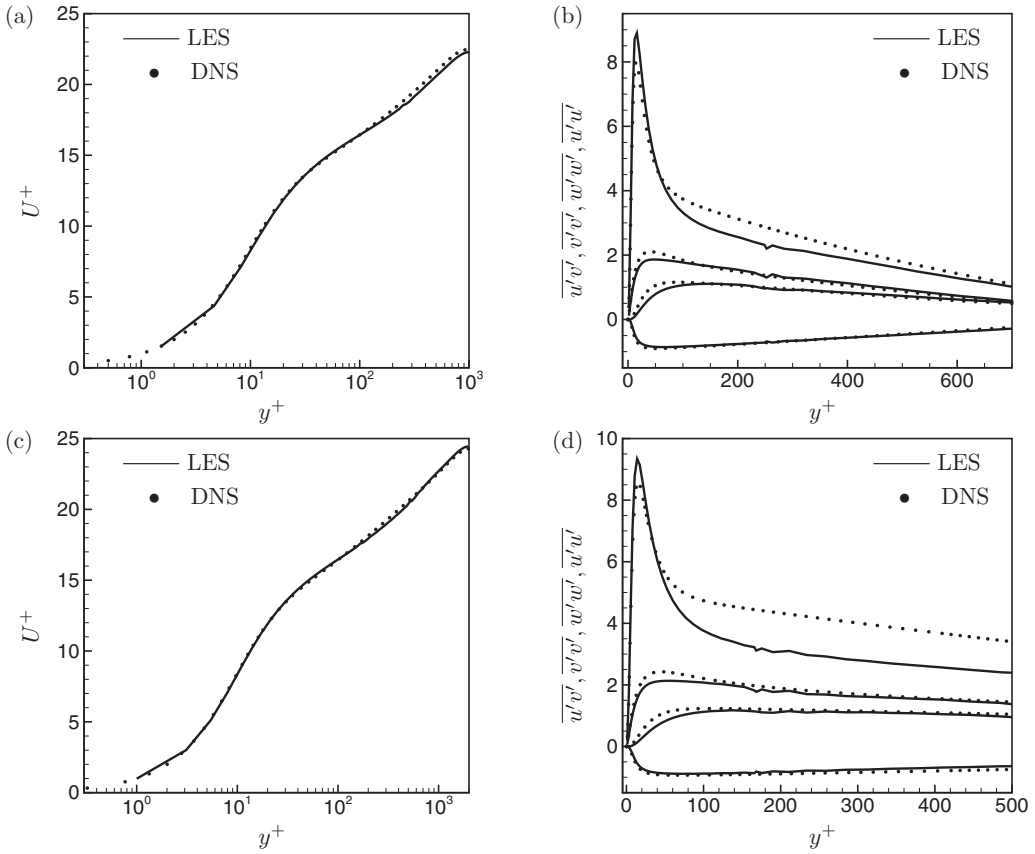

FIG. 8. Turbulent channel flow. Case 1ktl: (a) mean velocity, (b) rms velocity fluctuations; Case 2ktl: (c) mean velocity, (d) rms velocity fluctuations.

which is to enable a wall-resolved LES. Hence, it has two transition layers to coarsen from a fine near-wall Δz to a coarser outer region Δz as listed in Table I. Figure 8 also shows good agreement for the mean velocity and rms velocity fluctuations with unfiltered DNS. These examples show that the Lagrangian DSM with T_{SC} also works well for high Reynolds numbers on unstructured grids.

Figure 9 compares the computed Lagrangian time scales, plotted in inner and outer scaling, for the three cases—590tl, 1ktl, and 2ktl which correspond to $Re = 590$, 1000, and 2000, respectively. Note that the grid away from the wall is similar in all the cases. As Reynolds number increases, the normalized surrogate correlations of the GIE increase, which results in increasing T^+_{SC} (Fig. 9(a)). This trend of increasing Lagrangian time scale is also consistent with the observations of Choi *et al.*[8] who noticed an increase in the time scale of Lagrangian streamwise velocity correlations with Reynolds number in their DNS of turbulent channel flow. The jumps correspond to the locations where the grid transitions ($y/\delta \sim 0.3$).

4. Comparison between different averaging methods

For a given problem, as the grid becomes finer, the results obtained using different averaging schemes for DSM tend to become indistinguishable from one another.[22] On a finer grid such as case 590f, the effect of averaging and Lagrangian averaging time scale is small. Hence, in what follows, results are shown for case 590c which is a very coarse grid but which shows difference between the different averaging schemes. For all the averaging runs considered, statistics are collected over $96\delta/u_\tau$. Figure 10(a) shows that the mean velocity shows increasingly improving agreement with DNS as the averaging scheme changes from averaging along homogeneous directions (plane) to Lagrangian averaging using T_{LDSM} and finally T_{SC}. Figure 10(b) shows that the rms velocity

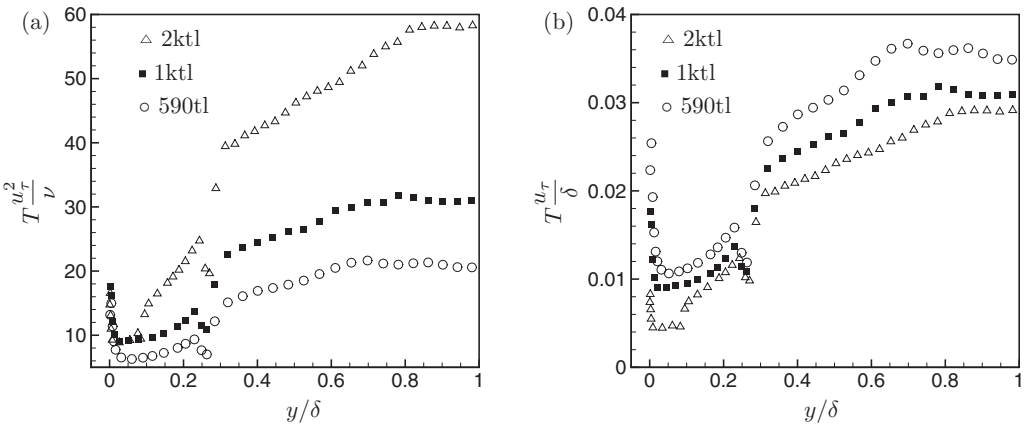

FIG. 9. Turbulent channel flow : Comparison of Lagrangian time scales T_{SC}. (a) scaled in viscous units T^+_{SC}, (b) scaled in outer units T_{SC}.

fluctuations are in a slightly better agreement with unfiltered DNS using T_{SC} over T_{LDSM}. $\overline{u'u'}$ is not plotted here as it is not much different for the two time scales. The fact that Lagrangian averaging performs better than plane averaging has been demonstrated by Meneveau *et al.*[6] and Stoll and Porté-Agel.[22] The present results show that using T_{SC} as the time scale for Lagrangian averaging can predict even better results.

Figures 10(c)–10(f) compare the differences between the time scales T_{SC} and T_{LDSM} in more detail. In general, increasing the extent of averaging by either increasing averaging volume (plane averaging) or increasing the averaging time scale (Lagrangian) will decrease the variance of the model coefficient. T_{LDSM} with $\theta = 3.0$ implies a larger averaging time scale than $\theta = 1.5$ and hence the eddy viscosity with $\theta = 3.0$ has a slightly lower mean and variance (Figs. 10(c) and 10(d)) when compared to $\theta = 1.5$. The Lagrangian model with T_{SC} has a lower mean compared to T_{LDSM} and this is consistent with lower dissipation leading to higher resolved turbulence intensities shown earlier in Fig. 10(b). Figure 10(d) shows that T_{SC} produces an eddy viscosity field that has much less variation than T_{LDSM} but more than plane averaging.

Stoll and Porté-Agel[22] report that the Lagrangian averaged model using T_{LDSM} has approximately 8% negative values for ν_t compared to 40% for the locally smoothed (neighbor-averaged) model in their simulations of a stable atmospheric boundary layer. The percentage of time that negative ν_t values are computed is shown in Fig. 10(e). Plane averaged ν_t never became negative and hence is not plotted. Clearly, ν_t averaged using T_{SC} has the least amount of negative values up until $y^+ \sim 100$ (which contains 50% of the points). Even after $y^+ \sim 100$, percentage of negative ν_t values computed by T_{SC} is less than T_{LDSM} with $\theta = 1.5$. It is also observed that increasing θ reduced the number of negative values, as expected intuitively. Therefore, T_{SC} is able to achieve the smoothing effect of plane averaging while retaining spatial localization.

When the time scales are compared (10(f)), it is found that T_{SC} actually overlaps with T_{LDSM}, $\theta = 3.0$ for almost half the channel width. For this particular computation, $\theta = 3.0$ is therefore preferable to $\theta = 1.5$. This makes it entirely reasonable to suppose that other flows might prefer some other θ than just 1.5. The dynamic procedure proposed in this paper alleviates this problem.

Finally, computing a dynamic T_{SC} for Lagrangian averaging the DSM terms does not incur a significant computational overhead. For case 590c, the total computational time required for computing T_{SC} and then using it for Lagrangian averaging of the DSM terms is just 2% more than that when no averaging of the DSM terms is performed.

B. Flow past a cylinder

The Lagrangian DSM with dynamic time scale T_{SC} (Eq. (17)) is applied to flow past a circular cylinder. Cylinder flow is chosen as an example of separated and free-shear flow. Also, cylinder flow

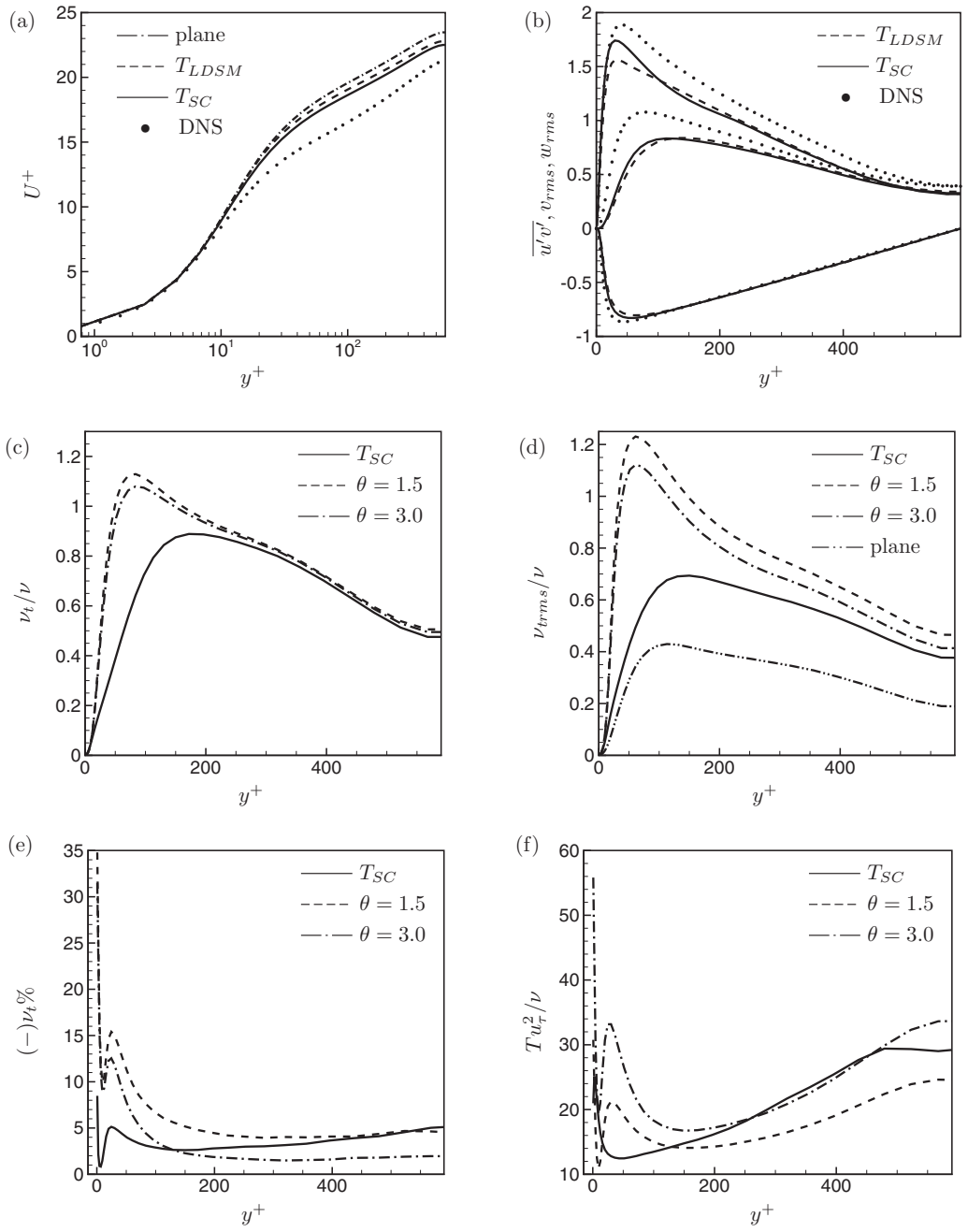

FIG. 10. Comparison of time scales from case 590c: (a) mean velocity, (b) rms velocity fluctuations, (c) mean eddy viscosity, (d) rms of eddy viscosity, (e) percentage of negative ν_t values, and (f) time scales.

varies significantly with Reynolds number, and is therefore a challenging candidate for validation. LES is performed at two Reynolds numbers (based on freestream velocity U_∞ and cylinder diameter D); $Re_D = 300$ and $Re_D = 3900$. The flow is transitional at $Re_D = 300$ and turbulent at $Re_D = 3900$. LES results are validated with available experimental data and results from past computations on structured and zonal grids at both these Reynolds numbers. An additional simulation is performed at $Re_D = 3900$ using time scale T_{LDSM} of Meneveau *et al.*[6] Results using T_{SC} are found to be in better agreement than using T_{LDSM}; the differences between the two time scales are discussed in Sec. IV B 5.

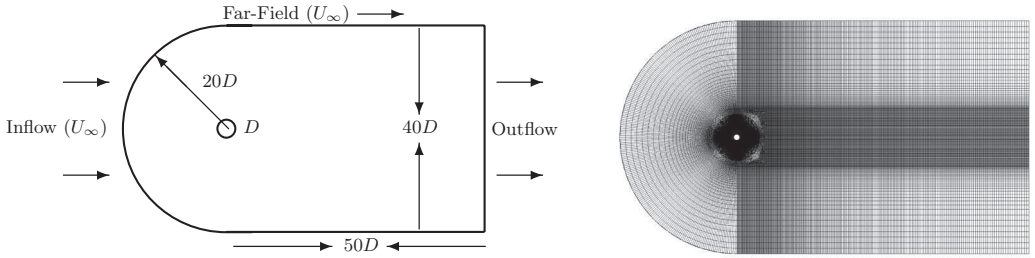

FIG. 11. Computational domain with boundary conditions and grid for a cylinder.

1. Grid and boundary conditions

The computational domain and boundary conditions used for the simulations are shown in Fig. 11. The domain height is $40D$, the spanwise width is πD and the streamwise extent is $50D$ downstream and $20D$ upstream of the center of the cylinder. An unstructured grid of quadrilaterals is first generated in a plane, such that computational volumes are clustered in the boundary layer and the wake. This two-dimensional grid is then extruded in the spanwise direction to generate the three-dimensional grid; 80 spanwise planes are used for both the simulations and periodic boundary conditions are imposed in those directions. Uniform flow is specified at the inflow, and convective boundary conditions are enforced at the outflow.

2. Validation at $Re_D = 300$

The $Re_D = 300$ computations are performed on a grid where the smallest computational volume on any spanwise station of the cylinder is of the size $2e^{-3}D \times 5.2e^{-3}D$ and stretches to $8.3e^{-2}D \times 8.3e^{-2}D$ at a downstream location of $5D$. Comparing this to the DNS of Mahesh,[17] his control volumes adjacent to the cylinder were of size $2.2e^{-3}D \times 1.0e^{-2}D$. As expected at this resolution, DSM is found to be dormant in the near-field. The wake of the cylinder is also well-resolved such that $\nu_t/\nu \sim 0.06$ even around $x/D = 30$. It can be safely assumed that SGS contribution from DSM is not significant in this case.

Integral quantities show good agreement with previous computations and experiment as shown in Table II. For comparison, the previous computations are the B-spline zonal grid method of Kravchenko *et al.*,[23] spectral solution of Mittal and Balachandar,[24] unstructured solution of Babu and Mahesh[25] and experimental results of Williamson.[26] Converged statistics are obtained over a total time of $360D/U_\infty$. Mean flow and turbulence statistics show excellent agreement with the spectral computations of Mittal and Balachandar[24] as shown in Fig. 12.

3. Validation at $Re_D = 3900$

The same computational domain as Fig. 11 and a similar grid topology is used to simulate turbulent flow past a cylinder at $Re_D = 3900$. The wake is slightly more refined than the $Re_D = 300$

TABLE II. Flow parameters at $Re_D = 300$. Legend for symbols: mean drag coefficient $\langle C_D \rangle$, rms of drag and lift coefficient ($\sigma(C_D)$, $\sigma(C_L)$), Strouhal number St and base pressure C_{P_b}.

	$\langle C_D \rangle$	$\sigma(C_D)$	$\sigma(C_L)$	St	$-C_{P_b}$
Current	1.289	0.0304	0.39	0.203	1.02
Kravchenko *et al.*[23]	1.28	...	0.40	0.203	1.01
Mittal and Balachandar[24]	1.26	...	0.38	0.203	0.99
Babu and Mahesh[25]	1.26	0.0317	0.41	0.206	...
Williamson[26]	1.22	...	...	0.203	0.96

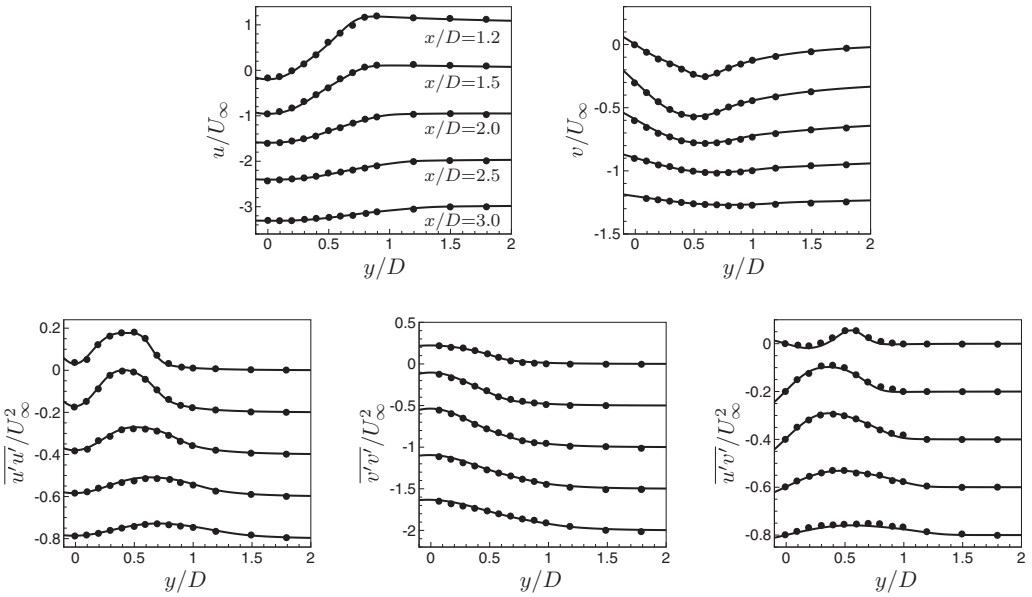

FIG. 12. Vertical profiles at streamwise stations downstream of the cylinder at $Re_D = 300$. —— : current solution; • : spectral solution of Mittal and Balachandar.[24]

grid. The smallest computational volume on any spanwise station of the cylinder is still of the size $2e^{-3}D \times 5.2e^{-3}D$ but stretches to $3.9e^{-2}D \times 2.9e^{-2}D$ at a downstream location of $5D$. To compare the performance of different Lagrangian averaging based methods, LES is performed using both the proposed dynamic time scale T_{SC} and time scale T_{LDSM} of Meneveau *et al.*[6] Integral quantities using T_{SC} show good agreement with the B-spline computation of Kravchenko and Moin[27] and the experiments of Lourenco and Shih (taken from Ref. 17) as shown in Table III. Note that T_{LDSM} also shows similar agreement for the wall quantities; however, L_{rec}/D which depends on the near-field flow, shows discrepancy. This points toward a difference in the values of the time scales away from the cylinder.

The time averaged statistics for flow over a cylinder have been computed by different authors using different time periods for averaging. Franke and Frank[28] studied this issue in detail and noted that more than 40 shedding periods are required to obtain converged mean flow statistics in the neighborhood of the cylinder. In the current work, statistics are obtained over a total time of $404D/U_\infty$ ($\sim$85 shedding periods) and then averaged over the spanwise direction for more samples. Converged mean flow and turbulence statistics using T_{SC} show good agreement with the B-spline computations of Kravchenko and Moin[27] and the experimental data of Ong and Wallace[29] up to $x/D = 10$ as shown in Figs. 13 and 14.

Results using T_{LDSM} are also shown for comparison. Difference in the statistics between the two time scales are seen to be significant in the near-wake up to $x/D \sim 4.0$, and decrease further downstream.

TABLE III. Flow parameters at $Re_D = 3900$. Legend for symbols : mean drag coefficient $\langle C_D \rangle$, rms of drag and lift coefficient ($\sigma(C_D)$, $\sigma(C_L)$), Strouhal number St and base pressure C_{P_b}, separation angle θ°_{sep}, and recirculation length L_{rec}/D.

	$\langle C_D \rangle$	$\sigma(C_L)$	St	$-C_{P_b}$	θ°_{sep}	L_{rec}/D
T_{SC}	1.01	0.139	0.210	1.00	88.0	1.40
T_{LDSM}	0.99	0.135	0.208	1.00	87.0	1.63
Kravchenko and Moin[27]	1.04	...	0.210	0.94	88.0	1.35
Lourenco and Shih (taken from Ref. 17)	0.99	...	0.215	...	86.0	1.40

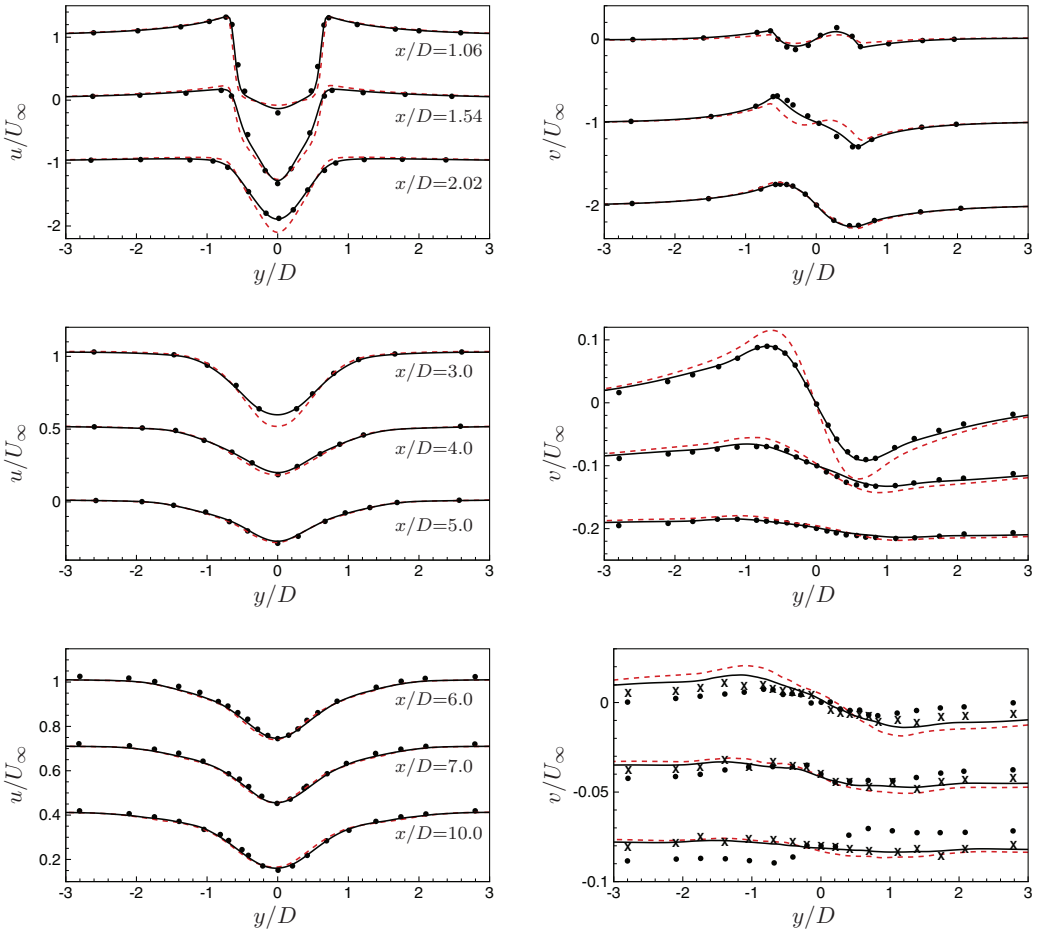

FIG. 13. Vertical profiles at streamwise stations downstream of the cylinder at $Re_D = 3900$. —— : T_{SC}; – – – – : T_{LDSM}; • : B-spline solution of Kravchenko and Moin;[27] × : Experiment of Ong and Wallace.[29]

The power spectral density (PSD) of streamwise, cross-flow velocity, and pressure at two downstream locations (x/D, y/D, z/D) ≡ (5, 0, 0), (10, 0, 0) are plotted in Fig. 15. Time history of u, v, p are obtained over an interval of $456D/U_\infty$ with 304 000 evenly spaced samples. The spectra are computed by dividing the time history into a finite number of segments with 50% overlap, applying a Hann window and rescaling to maintain the input signal energy. The frequency is non-dimensionalized by the Strouhal shedding frequency ω_{st}. The power spectra for u and v show good agreement with the experimental data of Ong and Wallace.[29] Consistent with previous studies,[27] the peaks in u are not very well-defined and so the p spectra are shown. The present LES shows peaks at twice the shedding frequency for the u and p spectra and peaks at the shedding frequency for v spectra, as expected at centerline locations of the wake. As noted by Kravchenko and Moin,[27] the spectra are consistent with the presence of small scales that remain active far from the cylinder and hence also consistent with the instantaneous flow shown in Fig. 16. They also noticed that the effect of excessive dissipation leads to a rapid decay of the spectra at the higher wave numbers and that spectra obtained by LES based on non-dissipative schemes better match the experiments. The agreement between current LES and experiment for a large spectral range, especially at high frequencies, confirms this trend while suggesting that the SGS model is not overly dissipative. At $x/D = 5$, the highest frequency from the current LES which matches the experiment is almost three times that of Kravchenko and Moin[27] while at $x/D = 10$, it is almost the same. Note that decay in the PSD at $x/D = 10$ is faster than the upstream location, consistent with coarsening streamwise resolution downstream.

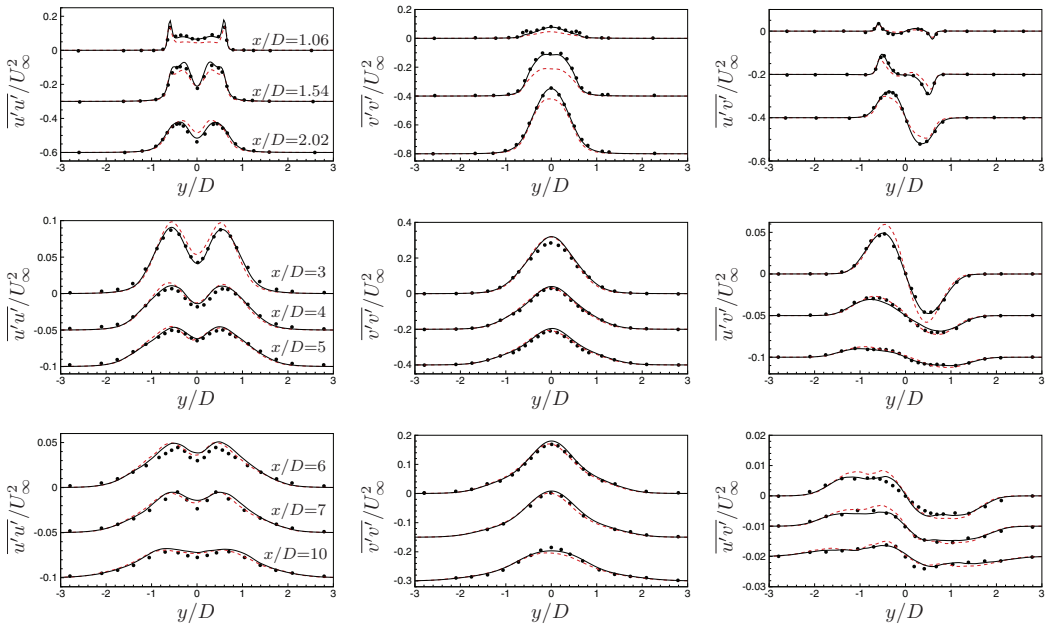

FIG. 14. Vertical profiles at streamwise stations downstream of the cylinder at $Re_D = 3900$. —— : T_{SC}; – – – – : T_{LDSM}; • : B-spline solution of Kravchenko and Moin.[27]

4. Instantaneous flow and GIE

Three-dimensional flow structures of varying scale are observed in Fig. 16. The separating shear layer transitions to turbulence, breaking up into smaller spanwise structures which then mix in the primary Karman vortex. An unsteady recirculation region with small scales is trapped between the shear layers. The figure also shows quasi-periodic longitudinal vortical structures as observed by previous studies[23,31] that are associated with vortex stretching in the vortex street wake.[31] Figure 17 shows that the instantaneous GIE also follows the pattern of the Karman vortex street. The top shear layer can be seen to roll up (within one diameter) to form the primary vortex. The GIE is highest in the turbulent shear layers where scales are smaller. As the grid becomes coarser downstream, DSM plays a more dominant role, providing a higher value of ν_t which reduces GIE. Note that GIE follows the dominant structures in the flow and hence it is reasonable that Lagrangian averaging uses a time scale based on a correlation of the GIE.

5. Comparison between T_{SC} and T_{LDSM}

The differences between statistics computed using T_{SC} and T_{LDSM} can be attributed to the contribution of the SGS model. Typically, in the near wake of the cylinder (up to $x/D \sim 2$), the cross-extent of eddy viscosity is within two diameters but the peak value around the centerline is still significant (Fig. 18). It spreads beyond three diameters after $x/D = 5$ and has a significant impact on the computed flow at $x/D = 10$ and beyond. Figures 18 and 19 also show differences in the computed eddy viscosity using different Lagrangian time scales. Eddy viscosity computed using T_{LDSM} (dashed) is consistently higher than using T_{SC} (solid). This explains the underprediction of the mean u-velocity in the near-field and hence the overprediction of the recirculation region (L_{rec}/D in Table III) using T_{LDSM}. Figure 19 shows that the centerline eddy viscosity is significant in the near wake and keeps increasing almost linearly with downstream distance after $x/D = 10$. The centerline eddy viscosity computed using T_{LDSM} is also greater than that using T_{SC} for $x/D > 1.5$. Hence increased accuracy of the results using T_{SC} could be attributed to reduced eddy viscosity in the shear layer. A similar observation was also made by Meneveau *et al.*[6] attributing the improved accuracy of Lagrangian averaging over the plane averaged dynamic model for channel flow to reduced eddy viscosity in the buffer layer.

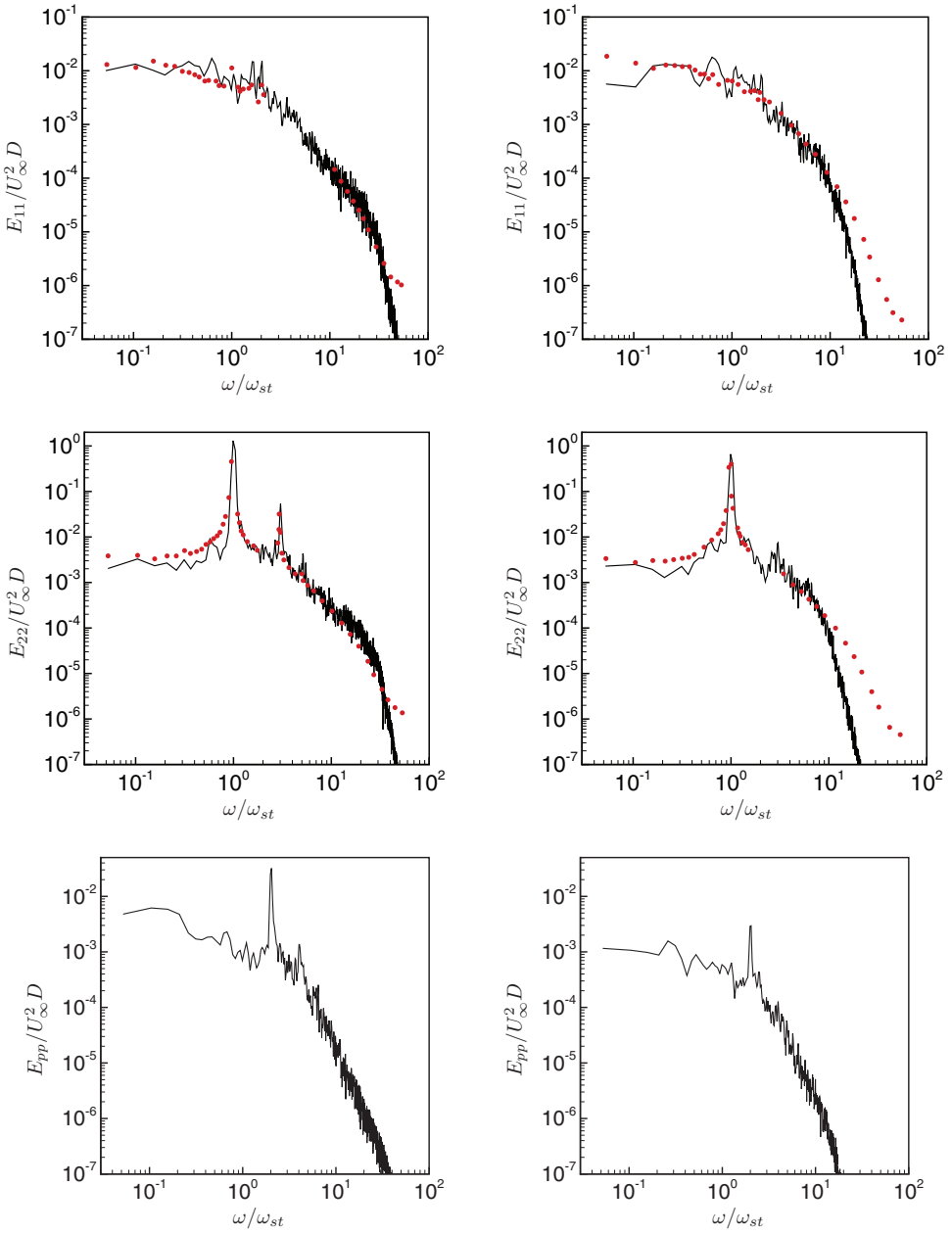

FIG. 15. Power spectral density at $x/D = 5.0$ (left), $x/D = 10.0$ (right); —— : current LES, • : experiment of Ong and Wallace .[29]

Differences in the computed eddy viscosity arise due to different time scales for Lagrangian averaging of the DSM terms. Both T_{SC} and T_{LDSM} are found to increase almost linearly downstream after $x/D > 5$ as shown in Fig. 20, though for different reasons. Based on the surrogate correlation of the GIE, increasing T_{SC} is consistent with the flow structures becoming bigger as they advect downstream. Whereas, the strong dependence of T_{LDSM} on the strain rate though $\mathcal{I}_{LM}$ and $\mathcal{I}_{MM}$ gives it a linear profile both ahead of and behind the cylinder. It can be argued that perhaps a different value of the relaxation factor θ would be more appropriate for this flow. In fact, Fig. 20 suggests scaling the value of θ by a factor of two or so ($\theta \geq 3.0$) will result in T_{LDSM} being close to T_{SC} after $x/D > 5$. Recall that for turbulent channel flow (end of Sec. IV A), T_{SC} actually overlaps with T_{LDSM}, $\theta = 3.0$ for almost half the channel width, therefore suggesting $\theta = 3.0$ to be a preferable alternative

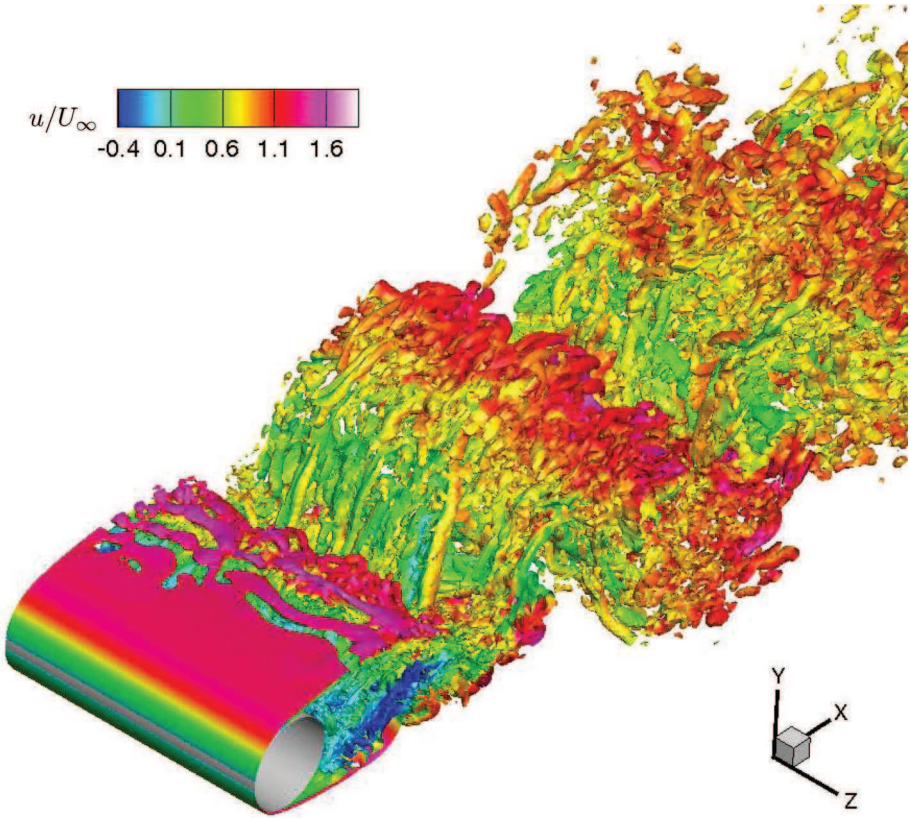

FIG. 16. Cylinder flow - $Re_D = 3900$: instantaneous iso-surfaces of Q-criterion[30] ($Q = 2$) colored by u-velocity.

to $\theta = 1.5$. However, it is clear that T_{LDSM} would still not show the appropriate trend ahead of the cylinder and in the recirculation region. Note that T_{SC} is high just behind the cylinder ($x/D \sim 1$) in the recirculation region and low in the high acceleration region ahead of the cylinder, as is to be expected on intuitive grounds.

When the variation in the cross-direction is considered (Fig. 21), T_{SC} is relatively high in the wake centerline which is consistent with the relatively low momentum flow directly behind the cylinder. T_{LDSM} shows the opposite behavior as it is low in the centerline, consistent with a higher strain rate. Again, this opposite trend cannot be changed by a different value of θ.

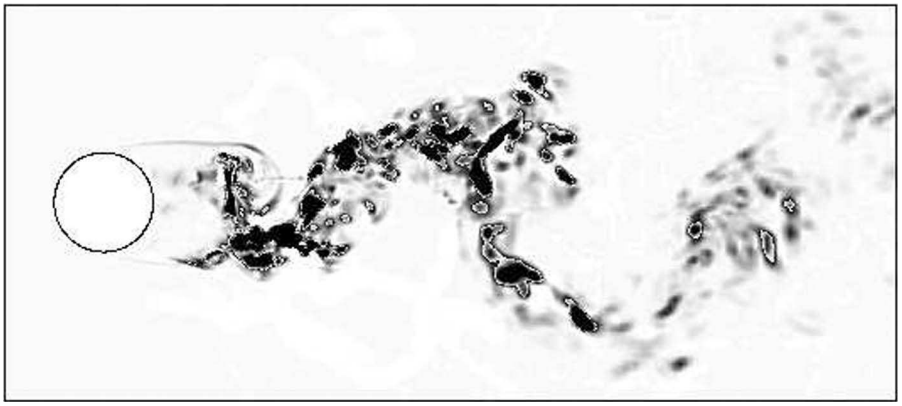

FIG. 17. Cylinder flow. $Re_D = 3900$: instantaneous contours of Germano-identity error whose contours vary as $0 \leq (\mathrm{GIE}/U_\infty^2)^2 \leq 0.001$.

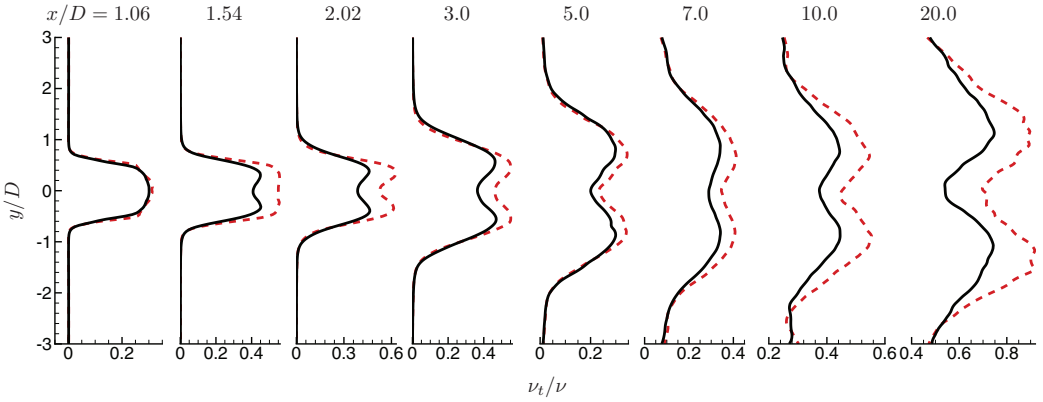

FIG. 18. Profiles of the mean eddy viscosity at streamwise stations in the cylinder wake at $Re_D = 3900$. —— : T_{SC}; – – – – : T_{LDSM}.

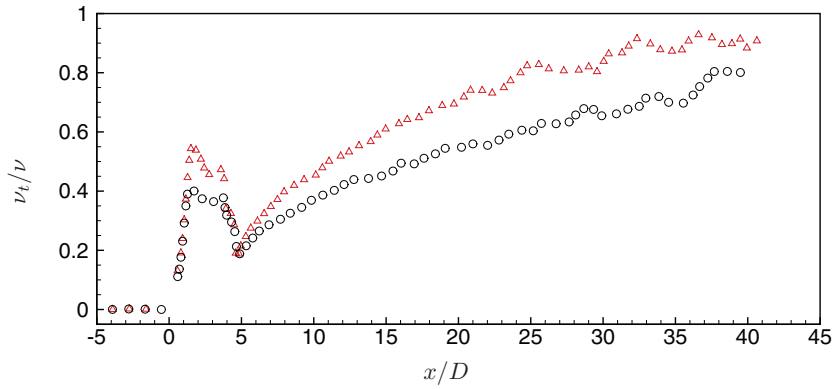

FIG. 19. Downstream evolution of the mean eddy viscosity on the centerline of the cylinder wake at $Re_D = 3900$. ○ : T_{SC}; △: T_{LDSM}.

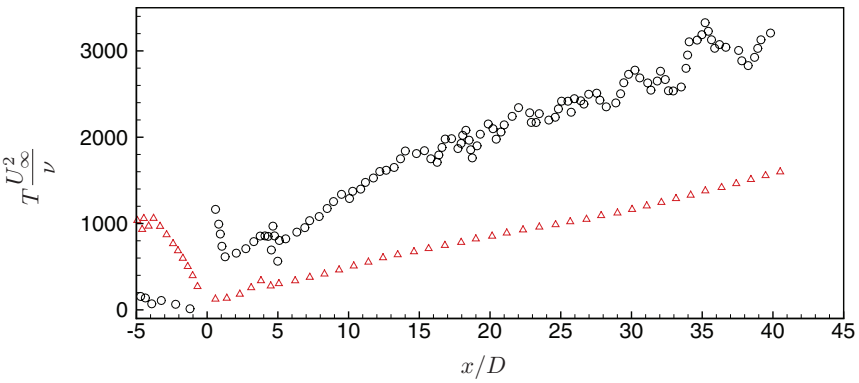

FIG. 20. Downstream evolution of the Lagrangian time scale on the centerline of the cylinder wake at $Re_D = 3900$. ○ : T_{SC}; △: T_{LDSM}.

C. Marine propeller in crashback

Propeller crashback is an off-design operating condition where the marine vessel is moving forward but the propeller rotates in the reverse direction to slow down or reverse the vessel. The crashback condition is dominated by the interaction of the free stream flow with the strong reverse flow from reverse propeller rotation; this interaction forms an unsteady vortex ring around the propeller. Crashback is characterized by highly unsteady forces and moments on the blades due to large

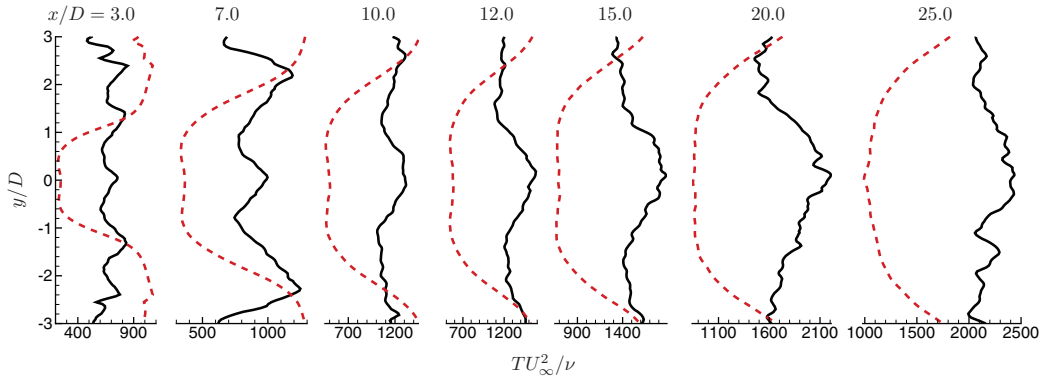

FIG. 21. Profiles of the Lagrangian time scale at streamwise stations in the cylinder wake at $Re_D = 3900$. ——: T_{SC}; – – – –: T_{LDSM}.

flow separation and hence is a challenging flow for simulation. Vyšohlíd and Mahesh[32,33] performed one of the first LES of a marine propeller in crashback. Chang *et al.*[34] coupled the unsteady blade loads with a structural solver to predict shear stress and bending moment on the propeller blades during crashback. Jang and Mahesh[35] studied crashback at three advance ratios and proposed a physical flow mechanism for unsteady loading. Verma *et al.*[36,37] explained the effect of an upstream hull on a marine propeller in crashback. These simulations were performed using locally-regularized DSM.

1. Simulation details

In the current work, LES of a marine propeller, attached to an upstream hull, is performed using the Lagrangian averaged DSM with the proposed dynamic time scale (Eq. (17)). Results are shown at a Reynolds number of $Re = 480\,000$ and advance ratio of $J = -0.7$. Here

$$Re = \frac{UD}{\nu} \quad \text{and} \quad J = \frac{U}{nD},$$

where U is the free-stream velocity, n is the propeller rotational speed, and D is the diameter of the propeller disk. The geometry of the propeller and hull are the same as in Bridges *et al.*[38]

Simulations are performed in a frame of reference that rotates with the propeller with the absolute velocity vector in the inertial frame. The computational domain is a cylinder with diameter $7.0D$ and length $14.0D$ as shown in Fig. 22(a). Free-stream velocity boundary conditions are specified at the inlet and the lateral boundaries. Convective boundary conditions are prescribed at the exit. Boundary conditions on the rotor part, blades, and hub are specified as $u = \omega \times r$, where $\omega = 2\pi n$ and r is the radial distance from the propeller center. No-slip boundary conditions are imposed on the hull body. An unstructured grid with 7.3×10^6 cvs is used as shown in Fig. 22(b). The propeller

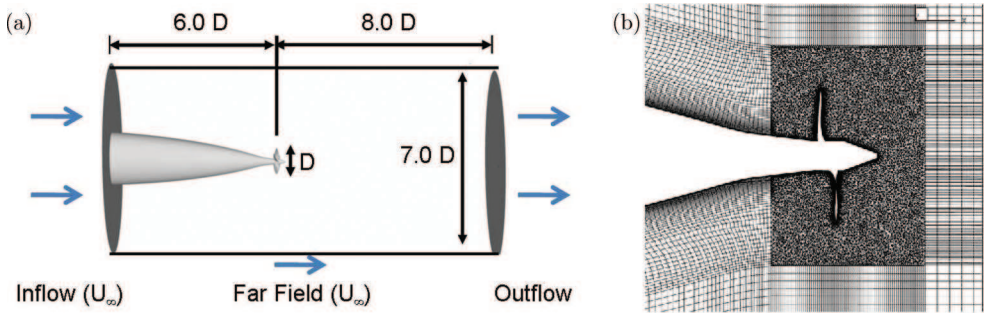

FIG. 22. (a) Computational domain and boundary conditions on domain boundaries, and (b) *XY* plane of grid for propeller with hull.

TABLE IV. Computed and experimental values of mean and rms of coefficient of thrust K_T, torque K_Q, side-force magnitude K_S, and rms of side-force K_F on propeller blades.

	$\langle K_T \rangle$	$\langle K_Q \rangle$	$\langle K_S \rangle$	$\sigma(K_S)$	$\sigma(K_F)$
LES	−0.358	−0.067	0.046	0.024	0.037
Expt.[a]	−0.340	−0.060	0.044−0.048	0.019−0.021	0.035−0.041

[a]Reference 38.

surface is meshed with quadrilateral elements. Four layers of prisms are extruded from the surface with a minimum wall-normal spacing of $0.0017D$ and a growth ratio of 1.05. A compact cylindrical region around the propeller is meshed with tetrahedral volumes while the rest of the domain is filled with hexahedral volumes.

The forces (axial T, horizontal F_H, and vertical F_V) and moments (axial Q) are non-dimensionalized using propulsive scaling as

$$K_T = \frac{T}{\rho n^2 D^4}, \quad K_H = \frac{F_H}{\rho n^2 D^4}, \quad K_V = \frac{F_V}{\rho n^2 D^4}, \quad K_S = \frac{\sqrt{F_H^2 + F_V^2}}{\rho n^2 D^4}, \quad K_Q = \frac{Q}{\rho n^2 D^5},$$

where ρ is the density of the fluid. Henceforth, $\langle \cdot \rangle$ denotes the mean value and $\sigma(\cdot)$ denotes standard deviation. RMS of the side-force is defined as

$$\sigma(K_F) = \frac{1}{2}\big(\sigma(K_H) + \sigma(K_V)\big).$$

2. Performance of T_{SC}

Time averaged statistics of flow field are computed over 70 propeller rotations. Table IV shows the predicted mean and rms of the unsteady forces and moments on the blades to be in reasonable agreement with the experiment of Bridges *et al.*[38] The time averaged flow statistics are further averaged along planes of constant radius to yield circumferentially averaged statistics in the $x - r$ plane; these are used in the subsequent discussion.

The idea of Lagrangian averaging for DSM was introduced by Meneveau *et al.*[6] to allow regularization of the DSM terms without resorting to averaging along homogeneous directions. The need for regularization becomes apparent in inhomogeneous flows such as the flow past a marine propeller. Figure 23(a) shows that if no averaging is performed for the DSM terms, large regions of the flow see negative eddy viscosities (ν_t) for more than 50% of the computed time steps. The negative ν_t values are more prevalent in the regions with unsteady flow, such as the ring vortex, wake of the hull, and the tetrahedral grid volumes in the vicinity of the propeller blades. On the other hand, Fig. 23(a) shows that regularization is achieved through Lagrangian averaging. The same unsteady regions of the flow experiencing negative ν_t values are greatly reduced.

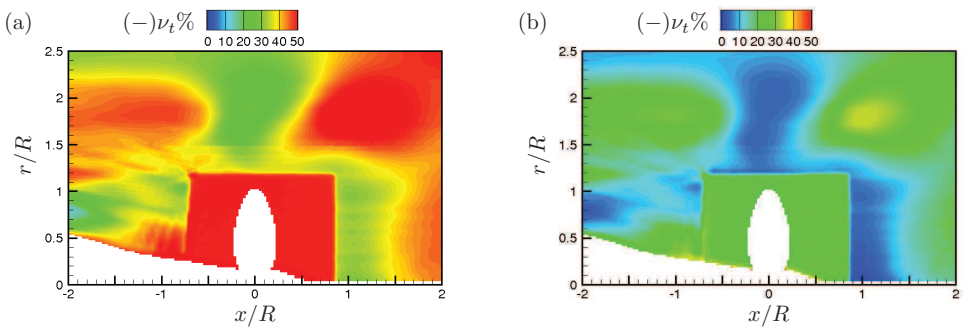

FIG. 23. Propeller in crashback. Percentage of negative values of eddy viscosity with (a) no averaging, and (b) Lagrangian averaging.

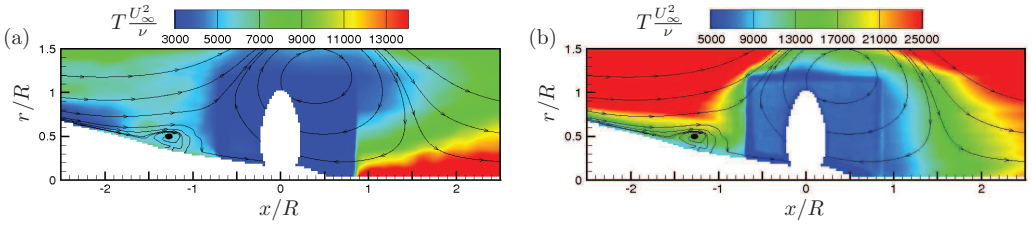

FIG. 24. Propeller in crashback. Contours of Lagrangian time scale with streamlines. (a) T_{SC}, and (b) T_{LDSM}.

Figure 24 compares the Lagranigan time scales T_{SC} and T_{LDSM}. Note that the computations are done using T_{SC} and T_{LDSM} is computed *a posteriori*. The streamlines reveal a vortex ring, centered near the blade tip. A small recirculation zone is formed on the hull ($x/R \sim -1.3$) due to the interaction of the wake of the hull with the reverse flow induced into the propeller disk by the reverse rotation of the propeller. Compared to $J = -1.0$,[37] this recirculation zone is smaller and located slightly upstream of the blades. This is consistent with a higher rotational rate of the propeller inducing a higher reverse flow into the propeller disk. The location of this recirculation region is intermediate to its locations at $J = -1.0$ and $J = -0.5$,[37] as would be expected.

T_{SC} is seen to be varying locally with the flow features. It is high in the low-momentum wake behind the propeller where flow structures are expected to be more coherent. It is low in the unsteady vortex ring region around the propeller blades. The cylindrical region around the blades is where the grid transitions from tetrahedral to hexahedral volumes. Interestingly, T_{SC} is higher in the small recirculation region on the hull. Whereas, T_{LDSM} does not show such level of local variation. It varies smoothly from low values on the hull body and the unsteady region around the propeller blades to higher values away from the propeller. The recirculation region on the hull and the propeller wake do not see a time scale much different from their neighborhood. The performance and physical consistency of T_{SC} for such complex flows is encouraging.

V. CONCLUSION

A dynamic Lagrangian averaging approach is developed for the dynamic Smagorinsky model for large eddy simulation of complex flows on unstructured grids. The standard Lagrangian dynamic model of Meneveau *et al.*[6] uses a Lagrangian time scale (T_{LDSM}) which contains an adjustable parameter θ. We extend to unstructured grids, the dynamic time scale proposed by Park and Mahesh,[12] which is based on a "surrogate-correlation" of the GIE. Park and Mahesh[12] computed their time scale for homogeneous flows by averaging along homogeneous planes in a spectral structured solver. The present work proposes modifications for inhomogeneous flows on unstructured grids. This development allows the Lagrangian averaged dynamic model to be applied to complex flows on unstructured grids without any adjustable parameter. It is shown that a "surrogate-correlation" of GIE based time scale is a more apt choice for Lagrangian averaging and predicts better results when compared to other averaging procedures for DSM. Such a time scale also removes the strong dependency on strain rate exhibited by T_{LDSM}. To keep computational costs down in a parallel unstructured code, a simple material derivative relation is used to approximate GIE at different events along a pathline instead of multi-linear interpolation.

The model is applied to LES of turbulent channel flow at various Reynolds numbers and relatively coarse grid resolutions. Good agreement is obtained with unfiltered DNS data. Improvement is observed when compared to other averaging procedures for the dynamic Smagorinsky model, especially at coarse resolutions. In the standard Lagrangian dynamic model, the time scale T_{LDSM} is reduced in the high-shear regions where $\mathcal{I}_{MM}$ is large, such as near wall. In contrast, the dynamic time scale T_{SC} predicts higher time scale near wall due to high correlation of GIE and this is consistent with the prevalence of near wall streaks. It also reduces the variance of the computed eddy viscosity and consequently the number of times negative eddy viscosities are computed.

Flow over a cylinder is simulated at two Reynolds numbers. The proposed model shows good agreement of turbulence statistics and power spectral density with previous computations and experiments, and is shown to outperform T_{LDSM}. The significance of using an appropriate Lagrangian time scale for averaging is borne out by significant difference in the computed eddy viscosity which consequently impact the results. Increased accuracy of the turbulent statistics using the proposed model can be attributed to reduced eddy viscosity in the shear layer. GIE is shown to follow the Karman vortex street and the behavior of the resulting time scale also shows consistency with the unsteady separation bubble, recirculation region, and increasing size of flow structures in the cylinder wake. Note that Park and Mahesh[12] found that, with their control-based corrected DSM, T_{SC} is lesser than T_{LDSM} in the center of a channel, which increases the weight of the most recent events, making their corrections more effective. This behavior of the time scales is opposite from what we observe from turbulent channel flow (case 590c) and also cylinder flow at $Re_D = 3900$. We observe that $T_{SC} > T_{LDSM}$ near the channel-wall, center, and in the cylinder wake; a higher time scale leads to lower mean eddy viscosity, leading to more resolved stress and hence improved results.

When the model is applied to flow past a marine propeller in crashback, T_{SC} provides the regularization needed for computing eddy viscosity without sacrificing spatial localization. It is also established that T_{SC} is physically consistent with the dominant flow features and produces results in good agreement with experiments. Finally, the extra computational overhead incurred by the proposed Lagrangian averaging is only 2% compared to the cost when no averaging is performed (for case 590c).

ACKNOWLEDGMENTS

This work was supported by the United States Office of Naval Research (ONR) under Grant No. N00014-05-1-0003 with Dr. Ki-Han Kim as technical monitor. Computing resources were provided by the Arctic Region Supercomputing Center of HPCMP and the Minnesota Supercomputing Institute.

[1] J. Smagorinsky, "General circulation experiments with the primitive equations: I. The basic experiment," Mon. Weather Rev. **91**, 99 (1963).
[2] M. Germano, U. Piomelli, P. Moin, and W. H. Cabot, "A dynamic subgrid-scale eddy viscosity model," Phys. Fluids A **3**(7), 1760 (1991).
[3] D. K. Lilly, "A proposed modification of the Germano subgrid-scale closure model," Phys. Fluids A **4**(3), 633 (1992).
[4] T. S. Lund, S. Ghosal, and P. Moin, "Numerical simulations with highly variable eddy viscosity models," *Engineering Applications of Large Eddy Simulations* (ASME, 1993), Vol. 162, pp. 7–11.
[5] S. Ghosal, T. S. Lund, P. Moin, and K. Akselvoll, "A dynamic localization model for large-eddy simulation of turbulent flows," J. Fluid Mech. **286**, 229 (1995).
[6] C. Meneveau, T. S. Lund, and W. H. Cabot, "A Lagrangian dynamic subgrid-scale model of turbulence," J. Fluid Mech. **319**, 353 (1996).
[7] C. Meneveau and T. S. Lund, "On the Lagrangian nature of the turbulence energy cascade," Phys. Fluids **6**, 2820 (1994).
[8] J. I. Choi, K. Yeo, and C. Lee, "Lagrangian statistics in turbulent channel flow," Phys. Fluids **16**, 779 (2004).
[9] R. Anderson and C. Meneveau, "Effects of the similarity model in finite-difference LES of isotropic turbulence using a Lagrangian dynamic mixed model," Flow, Turbul. Combust. **62**(3), 201–225 (1999).
[10] F. Sarghini, U. Piomelli, and E. Balaras, "Scale-similar models for large-eddy simulations," Phys. Fluids **11**(6), 1596–1607 (1999).
[11] R. Stoll and F. Porté-Agel, "Dynamic subgrid-scale models for momentum and scalar fluxes in large-eddy simulations of neutrally stratified atmospheric boundary layers over heterogeneous terrain," Water Resour. Res. **42**, W01409, doi:10.1029/2005WR003989 (2006).
[12] N. Park and K. Mahesh, "Reduction of the Germano identity error in the dynamic subgrid model," Phys. Fluids **21**, 065106 (2009).
[13] D. You, M. Wang, and R. Mittal, "A methodology for high performance computation of fully inhomogeneous turbulent flows," Int. J. Numer. Methods Fluids **53**(6), 947–968 (2007).
[14] M. Inagaki, T. Kondoh, and Y. Nagano, "A mixed-time-scale SGS model with fixed model-parameters for practical LES," *Engineering Turbulence Modeling and Experiments* (Elsevier, 2002), Vol. 5, pp. 257–266.
[15] O. V. Vasilyev, G. De Stefano, D. E. Goldstein, and N. K.-R. Kevlahan, "Lagrangian dynamic SGS model for stochastic coherent adaptive large eddy simulation," J. Turbul. **9**, N11 (2008).
[16] A. L. Rovelstad, R. A. Handler, and P. S. Bernard, "The effect of interpolation errors on the Lagrangian analysis of simulated turbulent channel flow," J. Comput. Phys. **110**(1), 190–195 (1994).
[17] K. Mahesh, G. Constantinescu, and P. Moin, "A numerical method for large-eddy simulation in complex geometries," J. Comput. Phys. **197**(1), 215 (2004).

[18] H. Jang, "Large eddy simulation of Crashback in marine propulsors," Ph.D. dissertation, University of Minnesota, 2011.
[19] R. D. Moser, J. Kim, and N. N. Mansour, "Direct numerical simulation of turbulent channel flow up to $Re_\tau = 590$," Phys. Fluids **11**, 943 (1999).
[20] J. C. del Alamo, J. Jimenez, P. Zandonade, and Robert D. Moser "Scaling of the energy spectra of turbulent channels," J. Fluid Mech. **500**, 135–144 (2004).
[21] S. Hoyas and J. Jimenez, "Scaling of the velocity fluctuations in turbulent channel flow up to $Re_\tau = 2003$," Phys. Fluids **18**, 011702 (2006).
[22] R. Stoll and F. Porté-Agel, "Large-eddy simulation of the stable atmospheric boundary layer using dynamic models with different averaging schemes," Boundary-Layer Meteorol. **126**, 1–28 (2008).
[23] A. G. Kravchenko, P. Moin, and K. Shariff, "B-Spline method and zonal grids for simulations of complex turbulent flows," J. Comput. Phys. **151**(2), 757–789 (1999).
[24] R. Mittal and S. Balachandar, "On the inclusion of three dimensional effects in simulations of two-dimensional bluff body wake flows," *Proceedings of the ASME Fluids Engineering Division Summer Meeting, Vancouver, Canada* (ASME, 1997), p. 3281.
[25] P. Babu and K. Mahesh, "Aerodynamic loads on cactus-shaped cylinders at low Reynolds numbers," Phys. Fluids **20**, 035112 (2008).
[26] C. H. K. Williamson, "Vortex dynamics in the cylinder wake," Annu. Rev. Fluid Mech. **28**, 477 (1996).
[27] A. G. Kravchenko and P. Moin, "Numerical studies over a circular cylinder at $Re_D = 3900$," Phys. Fluids **12**(2), 403–417 (2000).
[28] J. Franke and W. Frank, "Large eddy simulation of the flow past a circular cylinder at $Re = 3900$," J. Wind. Eng. Ind. Aerodyn. **90**, 1191 (2002).
[29] L. Ong and J. Wallace, "The velocity field of the turbulent very near wake of a circular cylinder," Exp. Fluids **20**, 441–453 (1996).
[30] J. C. R. Hunt, A. Wray, and P. Moin, "Eddies, stream, and convergence zones in turbulent flows," Center for Turbulence Research Report No. CTR-S88, 1988.
[31] C. H. K. Williamson, J. Wu, and J. Sheridan, "Scaling of streamwise vortices in wakes," Phys. Fluids **7**, 2307 (1995).
[32] M. Vyšohlíd and K. Mahesh, "Large eddy simulation of propeller crashback," *Proceedings of Flow Induced Unsteady Loads and the Impact on Military Applications, Budapest, Hungary*, NATO Report No. RTO-MP-AVT-123, 2005, pp. 2-1–2-12.
[33] M. Vyšohlíd and K. Mahesh, "Large eddy smulation of crashback in marine propellers," *Proceedings of the 26th Symposium on Naval Hydrodynamics, Rome, Italy* (Office of Naval Research, 2006), Vol. 2, pp. 131–141.
[34] P. Chang, M. Ebert, Y. L. Young, Z. Liu, K. Mahesh, H. Jang, and M. Shearer, "Propeller forces and structural responses to crashback," *Proceedings of the 27th Symposium on Naval Hydrodynamics, Seoul, Korea* (Curran Associates, 2008), Vol. 2, pp. 1069–1091.
[35] H. Jang and K. Mahesh, "Large eddy simulation of marine propellers in crashback," *Proceedings of the 28th Symposium on Naval Hydrodynamics, Pasadena, California* (Curran Associates, 2010), Vol. 1, pp. 490–504.
[36] A. Verma, H. Jang, and K. Mahesh, "Large eddy simulation of the effect of hull on marine propulsors in crashback," *Proceedings of the 2nd International Symposium on Marine Propulsors, Hamburg, Germany*, edited by M. Abdel-Maksoud (Institute for Fluid Dynamics and Ship Theory, 2011), pp. 507–514.
[37] A. Verma, H. Jang, and K. Mahesh, "The effect of upstream hull on a propeller in reverse rotation," J. Fluid Mech. (to be published).
[38] D. H. Bridges, M. J. Donnelly, and J. T. Park, "Experimental investigation of the submarine crashback maneuver," J. Fluids Eng. **130**, 011103–1 (2008).